Nonvibrating granular model for a glass-forming liquid: Equilibration and aging

C. Tapia-Ignacio, J. Garcia-Serrano, and F. Donado
Instituto de Ciencias Básicas e Ingeniería, Universidad Autónoma del Estado de Hidalgo, Pachuca 42184, Hidalgo, Mexico
(Received 21 May 2016; revised manuscript received 1 September 2016; published 1 December 2016)

We studied experimentally a model of a glass-forming liquid on the basis of a nonvibrating magnetic granular system under an unsteady magnetic field. A sudden quenching was produced that drove the system from a liquid state to a different final state with lower temperature; the latter could be a liquid state or a solid state. We determined the mean-squared displacement in temporal windows to obtain the dynamic evolution of the system, and we determined the radial distribution function to obtain its structural characteristics. The results were analyzed using the intermediate scattering function and the effective potential between two particles. We observed that when quenching drives the system to a final state in the liquid phase far from the glass-transition temperature, equilibration occurs very quickly. When the final state has a temperature far below the glass-transition temperature, the system reaches its equilibrium state very quickly. In contrast, when the final state has an intermediate temperature but is below that corresponding to the glass transition, the system falls into a state that evolves slowly, presenting aging. The system evolves by an aging process toward more ordered states. However, after a waiting time, the dynamic behavior changes. It was observed that some particles get close enough to overpass the repulsive interactions and form small stable aggregates. In the effective potential curves, it was observed that the emergence of a second effective well due to the attraction quickly evolves and results in a deeper well than the initial effective well due to the repulsion. With the increase in time, more particles fall in the attractive well forming inhomogeneities, which produce a frustration in the aging process.

DOI: 10.1103/PhysRevE.94.062902

I. INTRODUCTION

Particles forming a liquid move randomly because of their collisions with other particles. The temporal correlations fall very quickly as time progresses. For short time periods, it is claimed that particles have a ballistic behavior. After many collisions, in the long-time regime, the motion becomes random and the particle behavior is diffusive. These dynamics can also be observed in the motion of microscopic particles immersed in a liquid. This motion is the Brownian motion, which would be ballistic over a short-time period and diffusive for a long-time regime. To study the full dynamics of a Brownian particle, it is necessary to follow the particle with a time resolution on the order of 10^{-6} s and a spatial resolution on the order of a nanometer scale. It had not been possible to carry out such experiments. However, recently, the transition from the ballistic regime to the diffusive regime in Brownian motion has been addressed experimentally and discussed in Refs. [1–3]. In these papers, it is reported that a single particle is tracked by optical interferometric techniques while it is confined in an optical trap. It has been corroborated that mean-squared displacement follows the solution of the Langevin equation. Despite this progress, experimental study of short-time regimes of an ensemble of particles having Brownian motion remains challenging. Furthermore, the study of similar experiments in systems composed of smaller particles, such as molecules in a liquid, is beyond reach using current experimental techniques.

When a liquid is cooled quickly, it suffers a glass transition. The slow evolution of the glassy state, known as *aging*, is observed. In the glassy state, the system is out of thermodynamic equilibrium, and particles exhibit slowed-down dynamics [4–8]. A direct study of the dynamics and the structural characteristics of the aging process in the system is not possible because we cannot currently track such particles. From indirect experiments, mainly dispersion experiments, it has been observed that the system evolves into more ordered configurations driving it toward the thermodynamic equilibrium state, but not reaching it at experimental times.

The dynamic equivalence between atomic liquids and colloidal liquid has been studied in Refs. [9,10]. Thus, colloidal systems have been used to model glass-forming liquids. The particle configuration in a concentrated colloidal system experiment changes as a function of the particle concentration in a way similar to a molecular system presenting structural changes as the temperature is decreased [9,11–17]. Studying these systems allows us to comprehend some aspects that are not possible to study in actual molecular glass-forming liquids. In colloidal systems, particles can be tracked for long periods of time and with a resolution high enough to determine their diffusive behavior [18,19]. Thus, the dynamics and structural properties can be studied directly from particle positions. In addition, granular systems have been used to model molecular glass-forming liquids [20,21]. Granular systems are composed of very large objects that can be observed macroscopically [22]. In some systems, the dynamics of the particles can be studied easily because their dynamics are relatively slow and can be tracked using standard methods to follow particles. Usually, a granular system is vibrated vertically [23–28], although some other mechanisms have been used to fluidize particle motions [29]. A useful characteristic of colloidal and granular systems for macroscopic models for glass-forming liquids is that interparticle interactions can be modulated by active controls.

We propose a method to carry out experiments to model Brownian particle motion and molecular motion using a nonvibrating granular system. In this system, the dimensionality is actually two-dimensional (2D), where the particle motions are constrained to the horizontal plane, in contrast with vertically vibrating systems in which the dimensionality is actually greater than 2D. Motions of the magnetizable particles are

achieved by exciting them with a sinusoidal magnetic field applied vertically. Although our system is dissipative because particles lose energy due to their interactions with the base of the container and through collisions with other particles, the lost energy is compensated for by the energy originating from the unsteady magnetic field. This energy input prevents particle motions from stopping, thus the system is not in thermodynamic equilibrium but in a stationary state.

We studied the equilibration and aging processes when the system is suddenly quenched from a liquid state to a final state with lower temperature, which could be in a fluid state or in a solid state. In our system, particles interact repulsively at long distances and attractively at short distances. Although we carried out several quenching experiments, we report in detail only three special cases that we consider to be representative of the dynamics and of the structural characteristics of the system. In particular, we observed the evolution of the system in the glass state with a temperature close to the glass-transition temperature. We describe the aging process in our system and the eventual frustration of this aging process, which occurs due to the emergence of spatial inhomogeneities arising from particle aggregation.

In Sec. II, we describe the experimental setup. In Sec. III, we study the effective temperature of the system. In Sec. IV, we show the behavior of the mean-squared displacement and the radial distribution function behavior for the different cases. In Sec. V, we analyze the experimental results in terms of the effective potential and the intermediate scattering function. Finally, in Sec. VI, we give our final comments and remarks.

II. EXPERIMENTAL SETUP

Our system was composed of 1000 stainless steel particles, ANSI 420 grade 1000, 1 mm in diameter, provided by Gimex SA. These particles were confined within a circular plate measuring 72 mm in diameter. The particle concentration is given by the surface fraction occupied by the particles, $\phi_s = 0.16$. The system was located horizontally in the middle of a pair of Helmholtz coils, 150 mm in diameter, which produce a homogeneous magnetic field perpendicular to the particle plane container. Figure 1 shows the experimental setup scheme. The coils were fed by a Kepco power amplifier driven by a PC controlled signal through a DAQ NI data acquisition card. The general form of the magnetic field B applied to our system was

$$B = B_c + B_o \sin(2\pi f t), \tag{1}$$

where B_c is a constant magnetic field of 35 G, B_o and f are the amplitude and the frequency of the unsteady part of the magnetic field, B_o takes values from 0 to 66 G, and f is kept at 9.25 Hz.

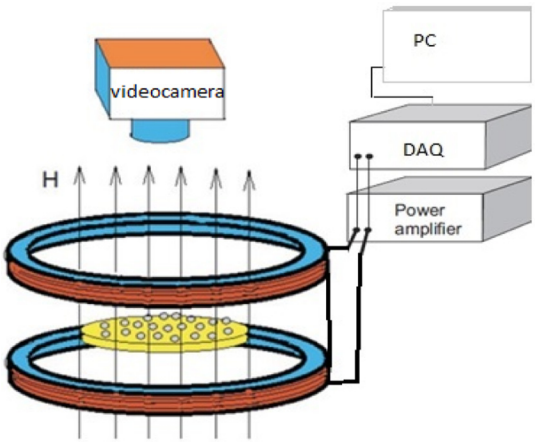

FIG. 1. Scheme of the experimental setup.

The experiments were recorded using a Sony HandyCam videocamera. The video files were taken at 30 fps in AVI interlaced format. From the videos, image sequences were obtained. During the decompression process, we used a filter to separate odd and even frames; thus, we obtained 1/60 s time resolution. By using ImageJ and its plugin Mosaic, we obtained the trajectories of the particles [30]. These trajectories were used to obtain the mean-square displacement $W(t)$ and intermediate scattering function $F(q\sigma,t)$ curves using programs we designed. We also obtained the radial distribution function $g(r)$ and the effective potential $U_E(r)$.

We measured the distances between the particles, and we determined that the minimum distance between two particles corresponds to the diameter σ of a particle. This means that the particles remain on the plane. This occurs because the mechanism for energy input that we use does not require vertically moving the plane. For comparison, in vibrating systems, the plane oscillates vertically to give the particles the opportunity to leave the plane and to move in three dimensions to randomize the motions. In our case, the particles never left the plane because the magnitude of the magnetic field was below a certain threshold. Thus, the motions are in two dimensions.

III. GRANULAR TEMPERATURE

In our experiments, the particles were subjected to a sinusoidal magnetic field all the time. The experiments were carried out after the magnetic field was turned on for one hour. After this period, we observed no further changes in the behavior of the system, at least not during the 300 s for each experiment. In that period, no changes in magnetization were expected. In experiments reported in Refs. [27,28], the particles were magnetized before the experiments were carried out, and no magnetic field was applied during the experiments. In those experiments, the plane on which the particles were located was vertically vibrated. In those cases, particle magnetization could not be retained because of the collisions and the friction. In our case, the unsteady component of the magnetic field randomized the particle motions while the steady component prevented them from forming chains and crystals, as was the case for those reported in Refs. [27,28]. The mechanism for the energy input and the randomizing of particle motion is described based on Fig. 2, which shows the scheme for a particle with a magnetic moment **m**. When a vertical sinusoidal magnetic field is turned on, the particle tends to align with the magnetic field to reach a minimum potential magnetic energy that is reached when $\alpha = 0$. Starting from a configuration where the particle is aligned in the sinusoidal magnetic-field direction, this field starts to decrease, and eventually it points in the opposite direction. In this new

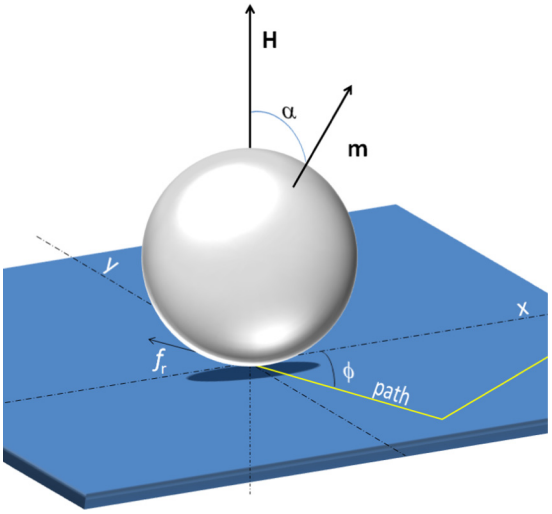

FIG. 2. Scheme of a sphere with a magnetic moment in a region with a vertical magnetic field. A trajectory and the parameters needed to describe the dynamics of the ball are shown.

condition, the magnetic energy of the particle in the magnetic field is not a minimum, and $\alpha = \pi$ rad. Thus, the particle rolls to align with the magnetic field again. The maximum energy that a magnetic particle in a sinusoidal magnetic field can receive can be obtained as follows. The magnetic potential energy of a magnetic dipole in a magnetic field is

$$U = -\mathbf{m} \cdot \mathbf{B} = -m[B_c + B_o \sin(2\pi f t)]. \tag{2}$$

Thus, the rate of change of energy in time is

$$\frac{dU}{dt} = -2\pi f m B_o \cos(2\pi f t). \tag{3}$$

Therefore, the maximum average change in energy of a particle in a period, considering the absolute values, is

$$\left\langle \frac{dU}{dt} \right\rangle = 4 m B_o f. \tag{4}$$

We observed that the energy input is linear in the frequency and in the amplitude of the unsteady part of the magnetic field. By contrast, in vibrating systems, previous research has shown that there is a complex and strong relationship between the energy input and the frequency and amplitude of the motion of the plane where the particles lie [31–33]. In some conditions, the energy input is proportional to the velocity plate [31]. In our experiment, not all the available energy, $4mB_of$, is transformed into the particle energy because of the friction f_r of the particles with the plane while rolling, and collisions with other particles; thus, we have a dissipative system. Although energy is quickly lost, it is compensated for by the energy originating from the unsteady magnetic field. This energy input prevents particle motions from stopping. Thus, the system is not in thermodynamic equilibrium; however, it can reach a stationary state.

Since a sphere has a neutral balance when it is on a horizontal plane, the rolling direction ϕ can take any possible value, and this is the origin of the randomizing of the motion. Although particle dynamics can be very complex, eventually the particle meets the initial condition described above and it can change its rolling direction to a new unpredictable direction. For high frequencies (greater than 30 Hz), there are no motions observed in most of the particles because of rotational inertia, and for low frequencies the motions are not continuous, as described in our experiments.

The density particle field is assured because the plane where the particles lie is horizontally leveled and no further motions are required for the plane. As previously described, the motions of the particles are random and the vertical magnetic field is homogeneous, and these factors assure a homogenization of the system.

In granular systems, to define an effective temperature the usual practice is to set $k_B = 1$. Thus, the equipartition theorem in a 2D system states that $\langle \frac{1}{2} m v^2 \rangle = T_E$, where T_E is the effective temperature, and the left term is the average particle kinetic energy. Such a definition of the effective temperature in terms of energy is also used in others reports, for instance in Ref. [27]. We also determined the T_E value through the Maxwell-Boltzmann velocity distribution,

$$f(v) = \frac{m}{T_E} v \exp\left(-\frac{m}{2T_E} v^2\right). \tag{5}$$

Figure 3 shows the values of the T_E as a function of the magnetic field B_o, which is our control parameter, obtained by using both methods. Figure 4 shows the Maxwell-Boltzmann distribution for different temperatures. In a vibrating granular system, the velocity distribution function depends strongly on the choice of the parameters used for randomizing particle motions. Thus, while some studies show that liquidlike states exhibit non-Maxwell-Boltzmann distributions [34–38], other studies show that under specific conditions, such as low particle concentration and a rough plate, the liquidlike states can have Maxwell-Boltzmann velocity distributions [23,39–41].

We have shown the equivalence in our system for the temperature obtained from the Maxwell-Boltzmann distribution and that obtained from the equipartition theorem. In a wide range of temperatures, we observed that the temperature

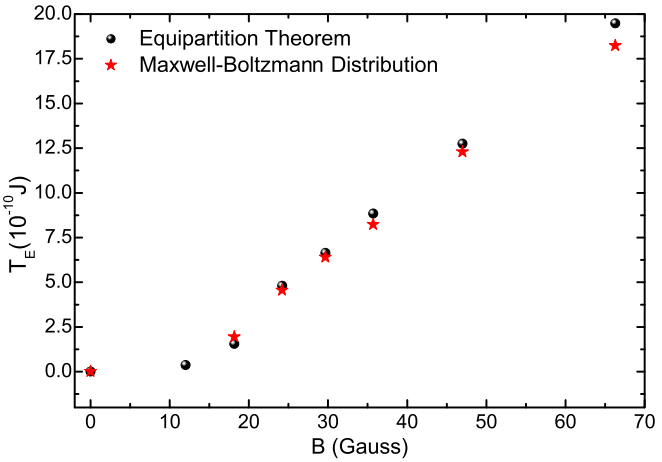

FIG. 3. Relation between the effective temperature T_E of the system as a function of the magnetic field, which is the control parameter in the system.

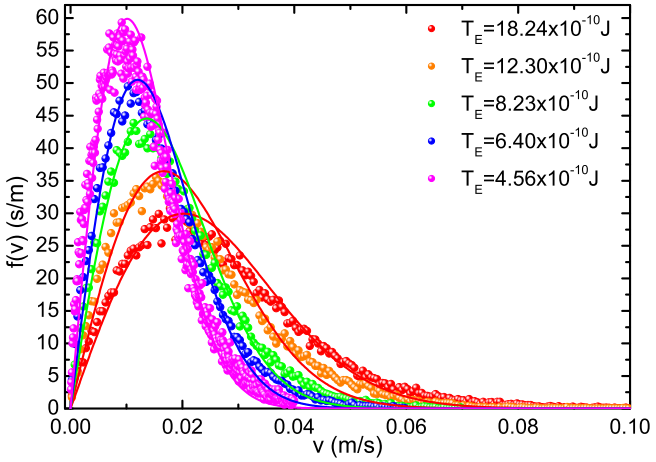

FIG. 4. Maxwell-Boltzmann velocity distribution for different temperatures. The labels indicate the effective temperature obtained from the fitting of the experimental data.

is proportional to the amplitude of the magnetic field, as suggested by Eq. (4).

IV. QUICK QUENCHING

We carry out quenching experiments from the same initial temperature to a final state with lower temperature. Figure 5 shows the behavior of the $W(t)$ curves obtained from the system, in a time window of 1.66 s immediately after the system was quenched. Each curve corresponds to a different final temperature. As expected, as the temperature decreases, the $W(t)$ values decrease. It is observed that for most of the time domain, the dependence of each $W(t)$ curve with time is linear, showing that particle motions are diffusive.

According to the Einstein relation in a diffusive 2D system, $W(t) = 4Dt$, where D is the diffusion coefficient. Figure 6 shows D values for the corresponding $W(t)$ curves shown in Fig. 5. As the temperature increases, the D values remain low until the temperature is higher than a threshold value, then

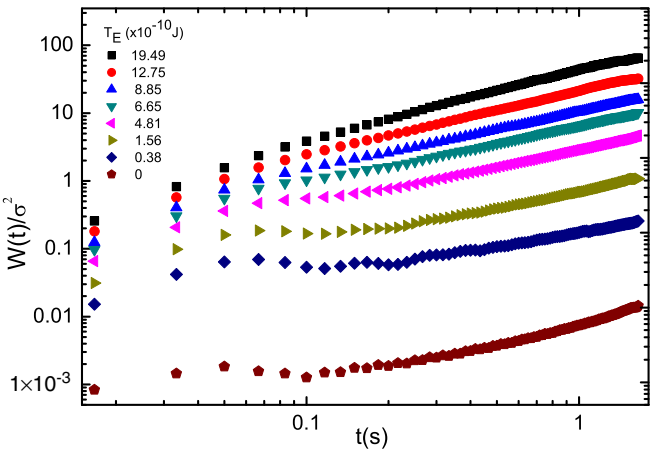

FIG. 5. $W(t)$ curves for several effective temperatures. Note the linear behavior of the curves corresponding to high temperature. We can observe that the emergence of a plateau indicates arrested behavior at low temperatures.

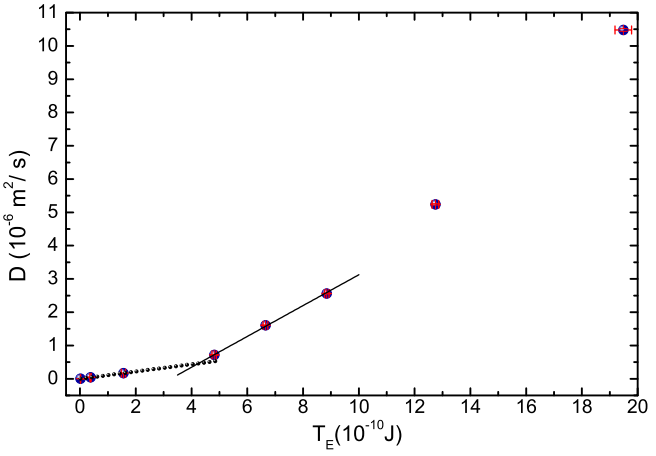

FIG. 6. Average diffusivity as a function of the effective temperature. The black continuous line is a linear fitting to D values corresponding to high temperatures. The dotted line is a linear fitting to D values corresponding to low temperatures.

the D values grow quickly as the temperature increases: this determines two temperature regimes, namely low and high regimes. We determined linear fitting curves for the D values in both the high- and low-temperature regimes, and then we determined their intersection, which is $T_g = 4.25 \times 10^{-10}$ J.

Figure 7 shows two typical trajectories observed in our system. Figure 7(a) shows trajectories corresponding to a system with a temperature above T_g. It is observed that the particles move around with a diffusive motion, modeling a liquid. Figure 7(b) shows arrested trajectories after a quick quenching where the final temperature is below T_g; in this case, it is observed that trajectories are confined, thus modeling a solid. Because the particles are confined in a disordered configuration, the system could be considered a model for glass. Thus, we observe a noticeable change in the behavior of the motion of the particles as the temperature of the system is decreased, from a total diffusive motion to a confined motion; therein we identify T_g as a glass-transition temperature.

According to the Stokes-Einstein equation, in a fluid, the effective viscosity is proportional to T_E/D. In Fig. 8, we plot $\log_{10}(T_E/D)$ as a function of T_g/T_E. We observe that the slowing down of the dynamics as the effective temperature approaches T_g is well described by a linear relationship. Therefore, the system shows Arrhenius law behavior; this behavior is characteristic of a *strong* glass-forming liquid. In Ref. [20], a vibrating granular system is shown that exhibits a slowing down of the dynamics that is described by the Vogel-Fulcher law; this characteristic is also presented by a *fragile* glass-forming liquid. Thus, depending on the mechanism for the input energy, a glass-forming liquid model on the basis of a granular system can exhibit a wide variation in fragility, such as that presented by a molecular glass-forming liquid or a colloidal glass-forming liquid [42]. In the following sections, we will provide additional arguments to support that there is a glass transition.

For the rest of the section, we analyze only three representative cases of quick quenching: cases A, B, and C. The initial temperature T_E for the three cases was 19.49×10^{-10} J. The

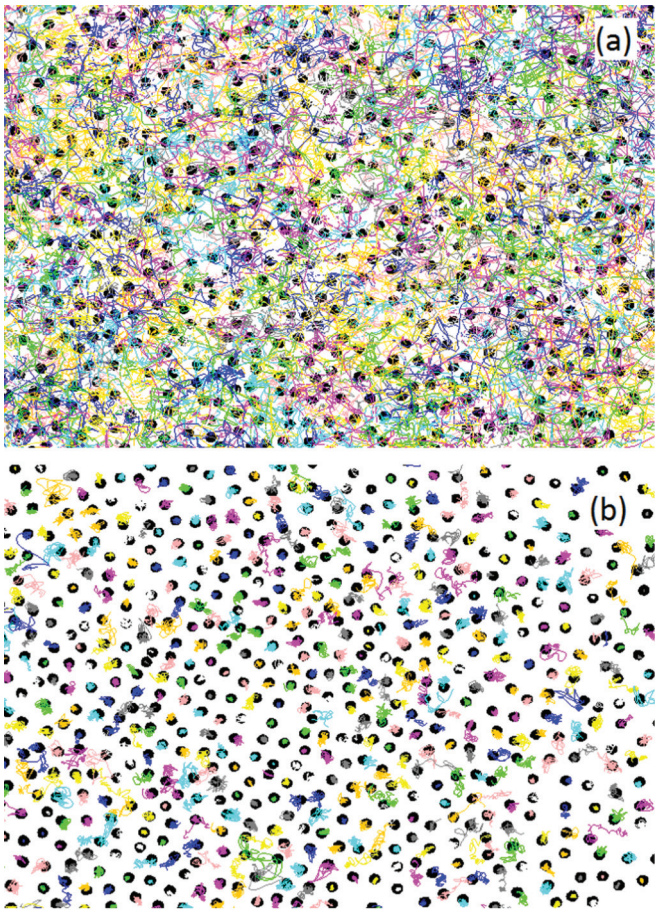

FIG. 7. Typical trajectories observed in the system. (a) Diffusive trajectories corresponding to a system with an effective temperature above the glass transition. (b) Arrested trajectories corresponding to a system with an effective temperature below the glass-transition temperature.

final temperatures T_E were 8.85, 1.56, and 0.00×10^{-10} J for cases A, B, and C, respectively. The glass-transition

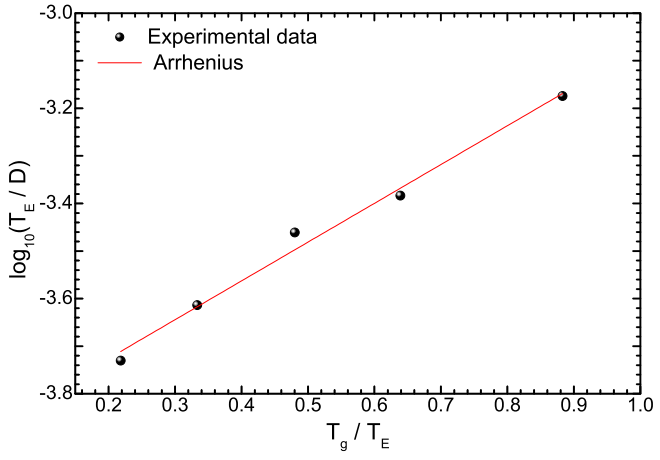

FIG. 8. Slowing down of the dynamics as the effective temperature approaches the glass-transition temperature. T_E/D is proportional to the effective viscosity. The solid line is a fit to the Arrhenius law.

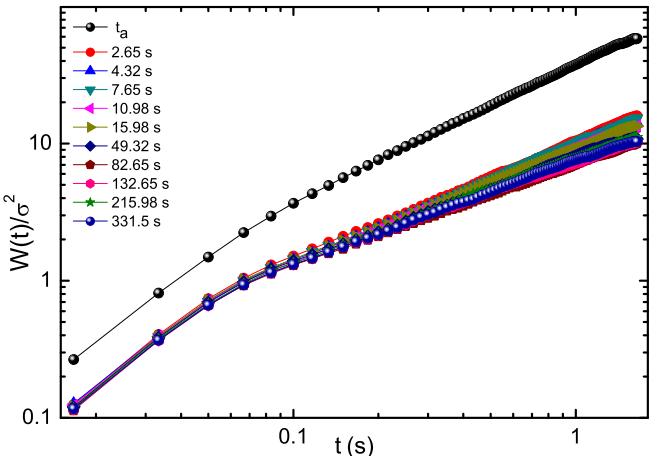

FIG. 9. $W(t)$ curves for several temporal windows after the quick quenching drives the system into a region where particles diffuse with lower energy. The curve labeled t_a corresponds to an initial high temperature before the quenching.

temperature T_g is $T_E = 4.25 \times 10^{-10}$ J. Figure 9 shows the behavior of the $W(t)$ curves for several temporal windows for case A. In this case, the final state is also a fluid state. Each temporal window takes 1.66 s and starts at a waiting time t_w. The waiting time is measured after the quick quenching. As expected, as t_w varies, the $W(t)$ curves quickly become similar and their values oscillate around an average value. The system evolves very quickly to the final state with lower energy. Figure 10 shows the radial distribution function for the same temporal windows. Here, we observe that the general behavior of the $g(r)$ curve shows liquidlike characteristics with a well-defined main peak: we will refer to it as $g(r)\max R$. Note that this peak arises around 1.7σ. This is because in this condition, the repulsion between particles dominates. When the system is cooled, the particle interactions are more effective in ordering local particles. Thus, the radial distribution function shows this tendency as an increase in $g(r)\max R$ values. Thus $W(t)$ and

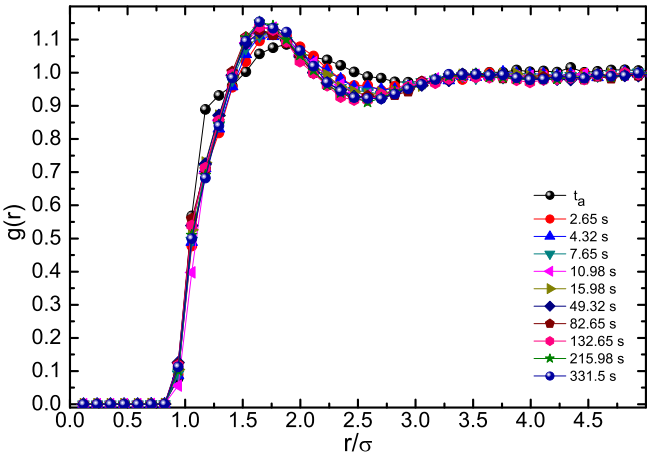

FIG. 10. Radial distribution function curves for several temporal windows. It can be seen that the curves reached stationary states very quickly. The curve labeled t_a corresponds to a state at high temperature, before the quenching.

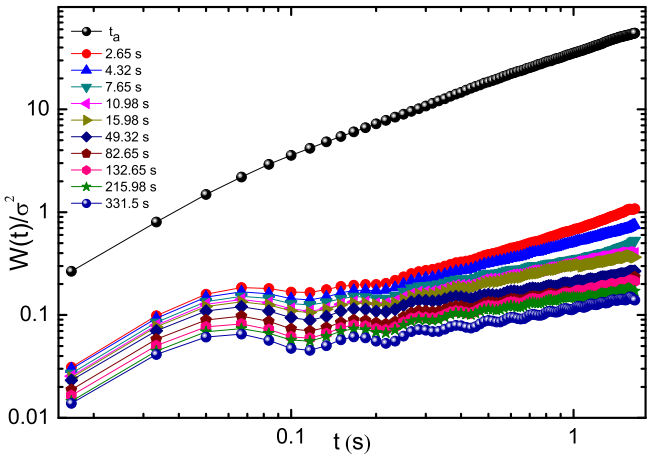

FIG. 11. $W(t)$ curves for several temporal windows for the case in which the system has an effective temperature below but near the glass transition. We can observe a relatively slow evolution of the curves. As time progresses, the $W(t)$ curves show lower displacement values. The curve labeled t_a corresponds to a state at high temperature before the quenching.

$g(r)$ curves show that the system evolves very quickly toward equilibration.

Case B is when the quenching drives the system into a final state with a temperature below the glass-transition temperature. Figure 11 shows the evolution of the $W(t)$ curves for this case. Although the trajectories are confined and show small $W(t)$ values, we can observe the slow evolution of the system into even lower $W(t)$ values. This means the system presents aging, i.e., it evolves slowly into more ordered states.

Figure 12 shows the $g(r)$ curves. First, there is an evolution toward a more ordered particle configuration reflected by the increase in the $g(r)\text{max}R$ values. However, we observe that at some point when t_w is in the range from 66 to 160 s, this evolution seems to stop and the system evolves in a

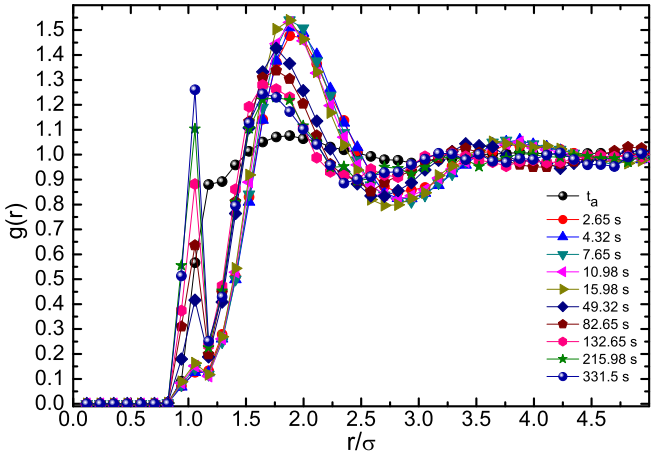

FIG. 12. Radial distribution function curves for several temporal windows. First, the $g(r)$ curves evolve to more ordered configurations; however, around 66 s they undergo a noticeable change, and a second peak starts to grow. The curve labeled t_a corresponds to the state at high temperature before quenching.

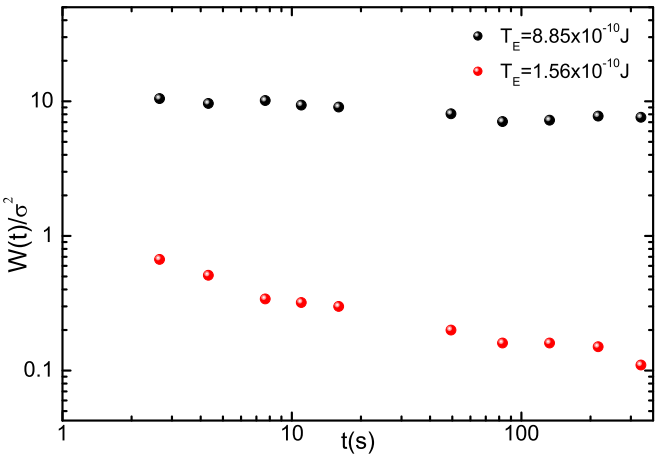

FIG. 13. Comparison of the mean-square displacement taken at 1 s as a function of the waiting time. For case B (see the text), aging is observed.

different way such that the $g(r)$ curves change noticeably. The $g(r)\text{max}R$ values, which were growing, start decreasing now. A new peak, $g(r)$maxHS, starts growing around one particle in diameter, and this peak increases with time as $g(r)\text{max}R$ decreases. In the next section, we will discuss this behavior in terms of the intermediate scattering function and the effective potential.

Figures 13 and 14 show a detailed comparison between cases A and B. Figure 13 shows $W(t)$ values taken at $t = 1$ s for different t_w values for cases A and B. For case A, when the final temperature after the quench is far above T_g, we observe almost no changes in the values for $W(t)$. For case B, even though the $W(t)$ are small, they show a clear tendency to decrease leading to aging. Figure 14 shows the evolution of $g(r)$ maximum values as a function of the waiting time for the two cases. For case A, the $g(r)\text{max}R$ values are almost constant, which means that the system quickly reaches a stationary state. For case B, we can observe that $g(r)\text{max}R$ values first increase and then decrease. The decreasing of $g(r)\text{max}R$ values coincides

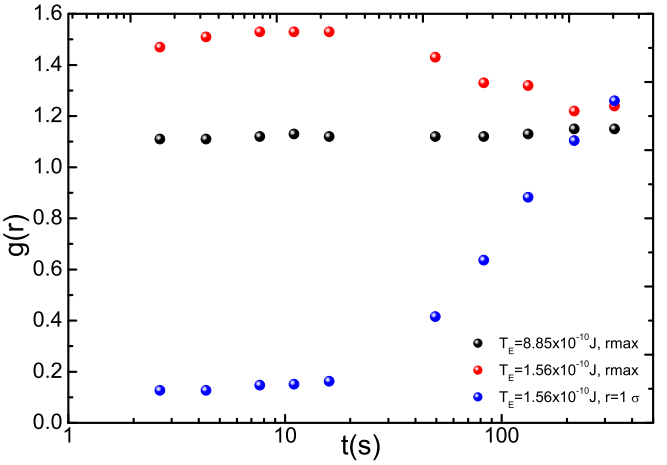

FIG. 14. Evolution of the peaks of the radial distribution function as a function of the waiting time for cases A and B. In case B there are two peaks, where one of them increases as the other decreases.

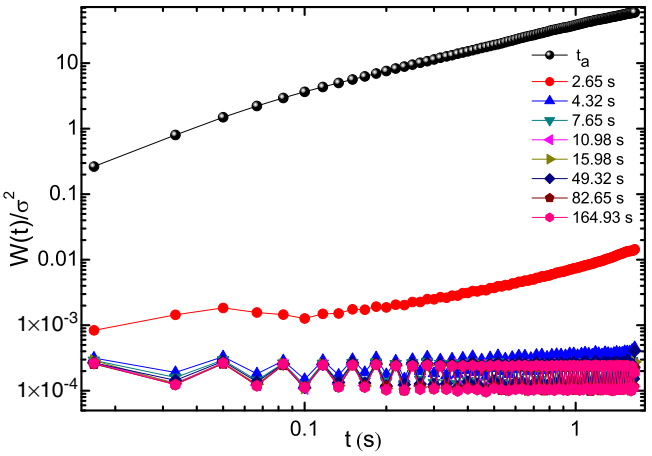

FIG. 15. $W(t)$ curves in the case in which the final temperature is zero. The curves immediately evolve to stationary states. The curve labeled t_a corresponds to a state at high temperature before the quenching.

with the increasing of the $g(r)$maxHS values. The formation of small aggregates can be observed from the experiments. Thus, the $g(r)$ peaks show that although the system presents aging, the initial mechanism of aging seems to be frustrated by the formation of stable aggregates. We will discuss this point more in depth in the next section when the effective potential is discussed.

The case C is when the system suffers a quick quenching that drives it into a state deep inside the arrested states zone. Figure 15 shows the $W(t)$ curves for this case where the final temperature is zero. Because the system started from a state of high energy and is then suddenly quenched, it takes some time to dissipate the energy; moreover, the particles continue moving without diffusion, but they are slightly vibrating. Note that the time window in our graph is about 2 s, and of course eventually the motion of the particles moves to zero.

Figure 16 shows the corresponding $g(r)$ curves. These $g(r)$ curves seem constant at least in the temporal scales that we studied. Thus, in this case, the system reaches a stationary state very quickly.

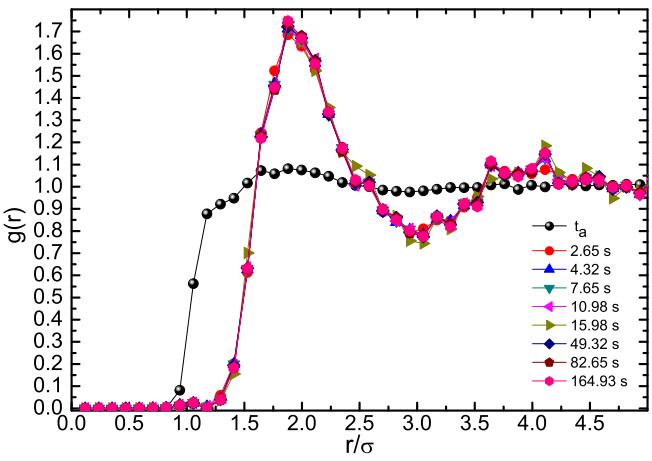

FIG. 16. The radial distribution function curves also evolve very quickly toward stationary states. The curve labeled t_a corresponds to a state at high temperature before the quenching.

V. ANALYSIS: EFFECTIVE POTENTIAL AND INTERMEDIATE SCATTERING FUNCTION

The effective potential curves give us information about the effective interactions among the particles in the dispersion. The general method that we follow to obtain the effective potential is described in Ref. [43]. It starts with a calculation of the radial distribution function $g(r)$, and then the total correlation function $h(r)$ is obtained. The direct correlation functions $c(r)$ and $h(r)$ are related using the Ornstein-Zernike equation

$$h(r_{12}) = c(r_{12}) + \rho \int d^3\mathbf{r}_3 c(r_{13}) h(r_{32}). \tag{6}$$

In the frequency space, using fast Fourier transform (FFT), this relation is transformed in

$$\hat{c}(k) = \frac{\hat{h}(k)}{1 - \rho\hat{h}(k)}. \tag{7}$$

After calculating $\hat{c}(k)$, one goes back to the real space by using the inverse FFT to obtain $c(r)$. The relationship between the $c(r)$ and the effective potential $U_E(r)$ is given in an approximate way by a closure relationship, for instance the Percus-Yevick (PY) or the hypernetted chain (HNC) approximations [44]. The PY approximation, in our case, is

$$c(r) = [h(r) + 1]\{1 - \exp[U_E(r)/T_E]\}. \tag{8}$$

The HNC approximation is given by

$$h(r) - c(r) = \ln g(r) + U_E(r)/T_E. \tag{9}$$

Both approximations can be solved for $U_E(r)$. We report results using both closure relations.

Another tool that we used is the scattering intermediate function $F(q\sigma,t)$, which for a homogeneous system is

$$F(q\sigma,t) = \left\langle \frac{\sin\{q[r_j(t) - r_j(0)]\}}{q[r_j(t) - r_j(0)]} \right\rangle. \tag{10}$$

$F(q\sigma,t)$ measures the temporal correlations of the particle positions. Based on the $F(q\sigma,t)$ curves, the α-relaxation time t_α is calculated determining the time that it takes the $F(q\sigma,t)$ to decay to $1/e$ from its initial value. When the decay is exponential, it is considered that at this time the diffusive motion starts. To determine the $F(q\sigma,t)$ curves, we use a particular value of the $\mathbf{q}$ at which the structure factor curve, not shown here, reaches its maximum value. Thus, for the initial case at high temperature, we use a $\mathbf{q}$ value, and after the quenching, because the structure had slightly changed, we use a second $\mathbf{q}$ value. If we use the same value of $\mathbf{q}$, the evolution of the $F(q\sigma,t)$ curves is similar.

Figure 17 shows $F(q\sigma,t)$ curves corresponding to different temporal windows for case A. We can see that the temporal correlations drop very quickly. This means the particle positions are time-uncorrelated and the motion is diffusive. The inset in Fig. 17 shows the α-relaxation time t_α as a function of the waiting time t_w. We can see that t_α evolves quickly toward a stationary state. Figure 18 shows the $U_E(r)/T_E$ curves for the system in this case. Both closure relationships give similar results. After the temperature drops, the system reaches a stationary state very quickly. The effective potential curves become practically constant as t_w grows. What we observed from the effective potential is that when particles

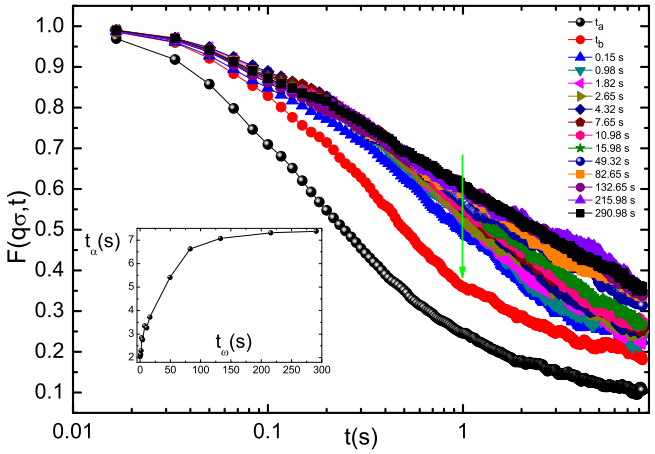

FIG. 17. $F(q\sigma,t)$ curves for several time windows after quenching starts. The curves exhibit a quick loss of temporal correlations. The curve labeled t_a corresponds to a state at high temperature before the quenching. The curve labeled t_b corresponds to a state at the initial position before quenching occurs, which undergoes quenching at the point indicated with the arrow. $q\sigma = 0.72$ for the t_a curve and $q\sigma = 0.65$ for the other curves.

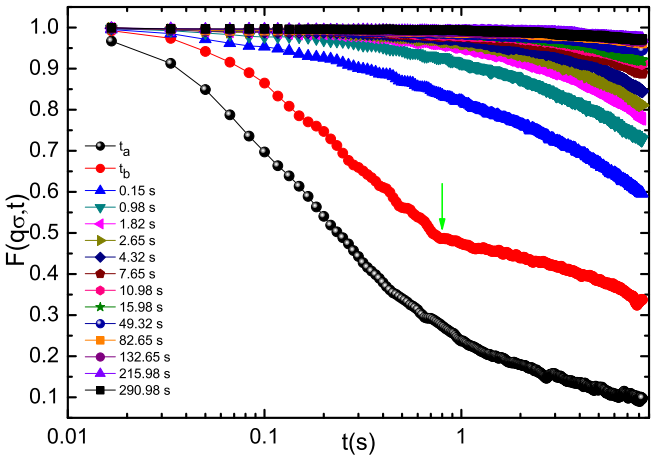

FIG. 19. $F(q\sigma,t)$ for the case in which the system is in the glassy state near the glass-transition temperature. The temporal correlation is lost; however, as the waiting time grows, the curves uncorrelate faster. The curve labeled t_a corresponds to a state at high temperature before the quenching. The curve labeled t_b corresponds to a state at the initial position before quenching occurs, which undergoes quenching at the point indicated by the arrow. $q\sigma = 0.75$ for the t_a curve and $q\sigma = 0.57$ for the other curves.

are near one another, they interact repulsively. This is because, on average, particle moments are oriented in the direction of the magnetic field, which is in the vertical direction. Thus, particles interact repulsively. We also observed a well around 1.5σ, indicating that the particles are weakly bound to positions where the energy is minimized even though the interactions are repulsive. We will refer to this well in the potential energy as $U_E(r)/T_E$-min$R$ because it corresponds to the peak radial distribution function $g(r)$max$R$. Thus this well due to repulsion among particles is equivalent to an effective attraction well. All particles push one another, compelling themselves to get closer. At long distances, the effective potential goes to zero because of the decay of the dipolar interactions and because of the randomizing of the motion. In videos, the formation of a few small aggregates can be observed, though they do not last long due to collisions with others particles.

Case B is when the system goes into the arrested region and still has enough energy to produce interesting behavior of the $F(q\sigma,t)$ and $U_E(r)/T_E$ curves. Figure 19 shows $F(q\sigma,t)$ curves for several temporal windows. Here this can be observed after the quenching particle positions are correlated. However, the curves also indicate that the system is not in an equilibrium state. It evolves to even more correlated motions. Figures 20 and 21 show the effective potential obtained after using the two closure relations described in the previous

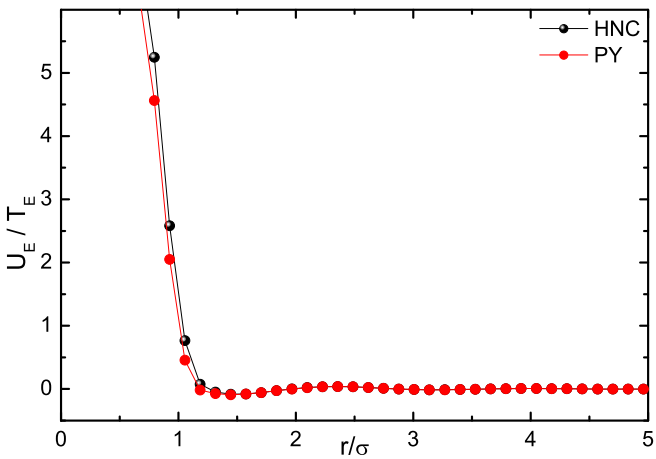

FIG. 18. $U_E(r)/T_E$ curves in the case in which the system falls into a state of lower effective temperature in a diffusive state. It can be seen that both approximations yield similar behavior. A weak well is observed of around 1.5 particle diameter. Of course, the repulsive part of the potential governs the dynamics of the system.

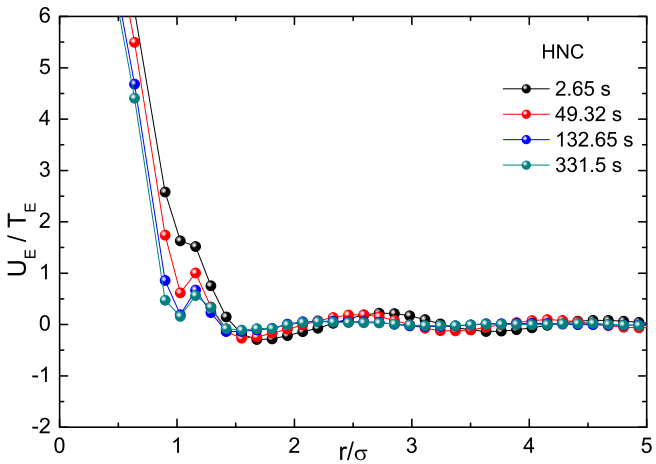

FIG. 20. $U_E(r)/T_E$ curves for different waiting times obtained using the HNC approximation in the case in which the system is near but below the glass transition. The growth and evolution of a second well of around one-particle diameter are observed, although values of the second well are all positive.

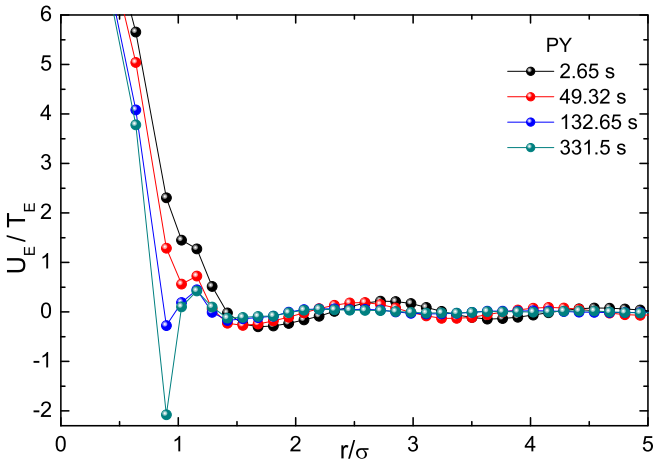

FIG. 21. $U_E(r)/T_E$ curves for different waiting times obtained using the PY approximation. The growth and evolution of a second well of around one-particle diameter is observed. Using this approximation, the second well takes values below the zero value.

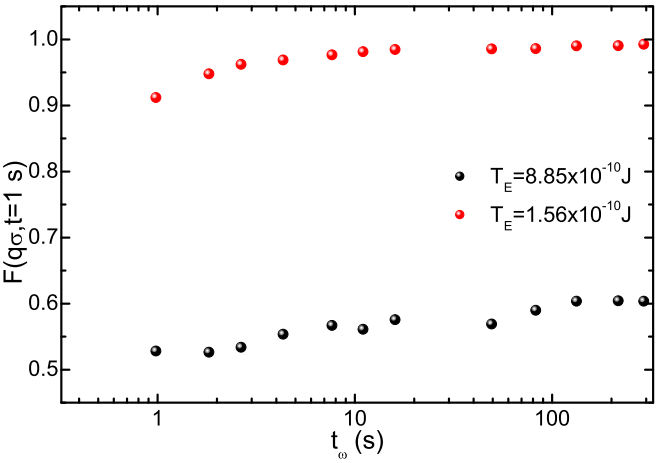

FIG. 22. $F(q\sigma,t)$ values taken at 1 s as a function of the waiting time. While in case A the values are low, in case B the values are almost the unit that shows high temporal correlation.

section. We have plotted them separately because in this case their behaviors are different.

Immediately after the quench occurs, the system falls into a state in which the particles occupy positions determined mainly by repulsive interactions. As we discussed above, in case A, particles push one another due to an effective well in the potential as if the interaction were attractive. It is observed in both figures that the well $U_E(r)/T_E$-min$R$ is around 1.5σ. As time progresses, the effective potential changes. Because of the attractive part of the actual potential, a second well, $U_E(r)/T_E$-minHS, arises. This well is observed at the same time in which some particles are aggregated. By this slow aggregation process, the system evolves locally toward configurations of less volume, and it becomes more inhomogeneous, as particle aggregation leaves empty spaces.

Comparing Figs. 20 and 21, one can observe that in both figures, the behavior to the right of $U_E(r)/T_E$-min$R$ is similar. However, the behavior to the left of $U_E(r)/T_E$-min$R$ is different. The effective potential differences become evident as time passes. In both approximations, the well $U_E(r)/T_E$-minHS, a well of around one-particle distance, can be observed. However, while in the HNC approximation the $U_E(r)/T_E$-minHS values are above the zero value, in the PY approximation the $U_E(r)/T_E$-minHS values evolve to negative values. In fact, this well becomes deeper than the $U_E(r)/T_E$-min$R$. At the beginning, the $U_E(r)/T_E$-minHS well is not observed; however, between 66 and 160 s after the beginning of the experiment, the well is formed and evolved. The well is developing very fast after around 160 s and becomes very deep. The picture is that obtained after the quench, where the particles rearrange locally. As time progresses, the system undergoes an aging process, where the peak $g(r)$max$R$ reaches higher values. However, the peak $g(r)$maxHS starts developing and the $g(r)$maxHS starts decreasing. This is because all particles push one another and compel themselves to get closer and closer, thereby producing enough energy to overcome the repulsions, and some particles enter the attraction well $U_E(r)/T_E$-minHS producing small aggregates. In these conditions, particles are more likely to interact through hard-sphere-like interactions than through long-range interactions. This is the reason the PY closure relation gives an effective potential that is more realistic than the HNC closure relation, according to what is observed in the experiments.

Figure 22 shows a comparison of the behavior of $F(q\sigma,t)$ values at 1 s as a function of the waiting time t_w for the two previous cases. For case A, the $F(q\sigma,t)$ values increase as the waiting time increases, and the values are from 0.5 to 0.8, meaning the temporal correlation at this time is almost lost. For the case B, on the other hand, the $F(q\sigma,t)$ values are almost stationary values near unity, meaning that the positions are highly correlated.

In case C, the system is quenched quickly from the maximum effective temperature to the lowest one. Figure 23 shows $F(q\sigma,t)$ curves for several temporal windows after

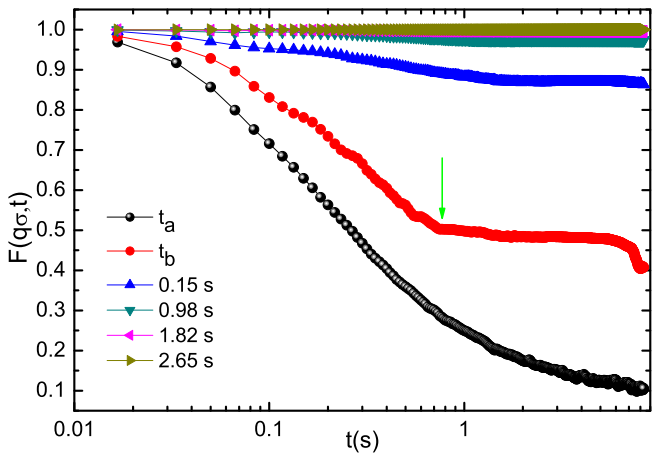

FIG. 23. $F(q\sigma,t)$ curves in the case in which the final effective temperature is zero. The curves are totally correlated because particles get arrested immediately. The curve labeled t_a corresponds to a state at high temperature before quenching. The curve labeled t_b corresponds to a state at the initial position before quenching occurs, which undergoes quenching at the point indicated by the arrow. $q\sigma = 0.72$ for the t_a curve and $q\sigma = 0.56$ for the other curves.

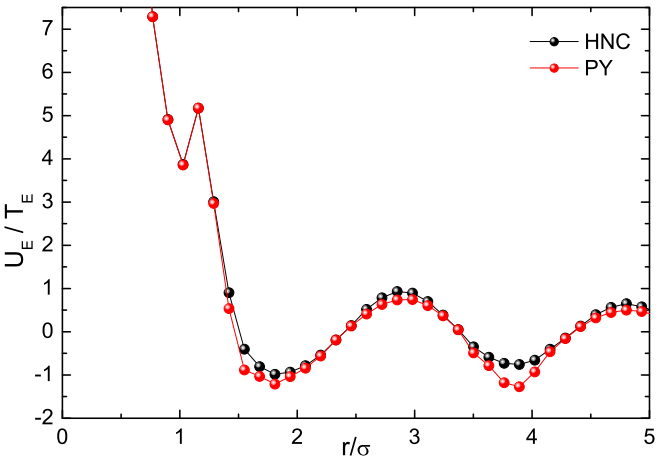

FIG. 24. $U_E(r)/T_E$ curve for the case in which the final temperature is zero. The effective potential shows a kind of periodic well.

quenching. It can be seen that the curves after the quench are almost the same. The particle positions are highly correlated because the motions practically stop. Figure 24 shows the corresponding effective potential in this case when the system goes deep into the arrested region. It can be observed that some effective wells are formed quickly and the system reaches an equilibrium state. Once the particles reach their arrested positions, it is very difficult to move them from those positions because they have low energy and their collective interactions are also small. It can be observed that the second well to the right is of the same depth as the first well. Both closure relations give similar effective potential curves.

VI. COMMENTS AND REMARKS

We studied a nonvibrating granular system to model quick quenching in a glass-forming liquid. This is a 2D system because the particle motions are always on the plane, in contrast to vibrating systems in which particle motions take place in a dimension that is effectively greater than 2. In this dissipative system, a constant input energy coming from the unsteady magnetic field prevents particles from stopping. The system reaches not a thermodynamic equilibrium state but rather a stationary one. The complex interactions of the particles with the field while they roll on produce particle motions that show diffusive behavior over a long time scale. We have used some tools commonly used in thermodynamic equilibrium systems in our stationary system to study some of these characteristics.

We carried out experiments in which quick quenching drives the system from an initial state in the liquid phase, where particles are diffusive and the density field is homogeneous, to final states with lower temperature. We observed that when the final state has high or very low energy, the system reaches quasiequilibrium states very quickly. When the final state is near the glass transition, the system shows an aging process. In this latter case, it is observed that the system falls into an arrested state due to the repulsive interactions and then it ages, changing its particle configurations toward lower energy states. However, after a waiting time, the $g(r)$ and the effective potential change noticeably. A second peak is developed in $g(r)$, in accordance with the formation of small aggregates as seen in the experiments. In the effective potential, the development of a well of around one-particle diameter corresponding to the attractive part of the actual pair potential between particles can be observed.

The collective interactions result in fluctuations that make some particles overcome the repulsive barrier and fall into the attractive well. As time progresses, this well becomes deeper than the well due to repulsive interactions. Particles fall in bound states where the bond energy is strong, and they form small stable aggregates. In this state, it is very difficult to observe that the aggregates break. When some particles fall into the attractive well, some space is released, and then the particles are rearranged and the main peak of $g(r)$ decreases. This aggregation process produces a frustration in the aging process. Finally, it is worth mentioning that the experimental setup could also be used to carry out other experiments in colloidal or molecular glass-forming liquids. For instance, such experiments could involve a cooling process that is carried out through a controlled ramp or dynamically tuning the interaction between the particles.

ACKNOWLEDGMENTS

We thank M. Medina-Noyola for very helpful discussions. Partial financial support by CONACyT-México through Soft Condensed Matter RED TEMATICA is acknowledged.

[1] P. N. Pusey, Science **332**, 802 (2011).
[2] T. Li, S. Kheifets, D. Medellin, and M. G. Raizen, Science **328**, 1673 (2010).
[3] R. Huang, I. Chavez, K. M. Taute, B. Lukić, S. Jeney, M. G. Raizen, and E. L. Florin, Nat. Phys. **7**, 576 (2011).
[4] L. Berthier and G. Biroli, Rev. Mod. Phys. **83**, 587 (2011).
[5] P. Ramírez-González and M. Medina-Noyola, Phys. Rev. E **82**, 061504 (2010).
[6] R. Casalini and C. M. Roland, Phys. Rev. E **69**, 062501 (2004).
[7] B. Charbonneau, P. Charbonneau, and G. Tarjus, Phys. Rev. Lett. **108**, 035701 (2012).
[8] J. P. Garrahan and D. Chandler, Proc. Natl. Acad. Sci. (USA) **100**, 9710 (2003).
[9] L. López-Flores, H. Ruíz-Estrada, M. Chávez-Páez, and M. Medina-Noyola, Phys. Rev. E **88**, 042301 (2013).
[10] P. E. Ramírez-González, L. López-Flores, H. Acuña-Campa, and M. Medina-Noyola, Phys. Rev. Lett. **107**, 155701 (2011).
[11] K. N. Pham, S. U. Egelhaaf, P. N. Pusey, and W. C. K. Poon, Phys. Rev. E **69**, 011503 (2004).
[12] B. Abou, D. Bonn, and J. Meunier, Phys. Rev. E **64**, 021510 (2001).
[13] E. H. Purnomo, D. van den Ende, S. A. Vanapalli, and F. Mugele, Phys. Rev. Lett. **101**, 238301 (2008).

[14] G. L. Hunter and E. R. Weeks, Rep. Prog. Phys. **75**, 066501 (2012).
[15] H. König, K. Zahn, and G. Maret, in *Slow Dynamics in Complex Systems: 3rd International Symposium on Slow Dynamics in Complex Systems*, edited by M. Tokuyama and I. Oppenheim, AIP Conf. Proc. No. 708 (AIP, New York, 2004), pp. 40–45.
[16] D. Bonn, S. Tanase, B. Abou, H. Tanaka, and J. Meunier, Phys. Rev. Lett. **89**, 015701 (2002).
[17] C. R. Nugent, K. V. Edmond, H. N. Patel, and E. R. Weeks, Phys. Rev. Lett. **99**, 025702 (2007).
[18] H. Acuña-Campa, M. D. Carbajal-Tinoco, J. L. Arauz-Lara, and M. Medina-Noyola, Phys. Rev. Lett. **80**, 5802 (1998).
[19] J. Santana-Solano, A. Ramírez-Saito, and J. L. Arauz-Lara, Phys. Rev. Lett. **95**, 198301 (2005).
[20] P. M. Reis, R. A. Ingale, and M. D. Shattuck, Phys. Rev. Lett. **98**, 188301 (2007).
[21] S. Merminod, M. Berhanu, and E. Falcon, Europhys. Lett. **106**, 44005 (2014).
[22] T. S. Majmudar, M. Sperl, S. Luding, and R. P. Behringer, Phys. Rev. Lett. **98**, 058001 (2007).
[23] G. W. Baxter and J. S. Olafsen, Granular Matter **9**, 135 (2007).
[24] M. Nicodemi and A. Coniglio, Phys. Rev. Lett. **82**, 916 (1999).
[25] X. Nie, E. Ben-Naim, and S. Y. Chen, Europhys. Lett. **51**, 679 (2000).
[26] A. Götzendorfer, C.-H. Tai, C. A. Kruelle, I. Rehberg, and S.-S. Hsiau, Phys. Rev. E **74**, 011304 (2006).
[27] D. L. Blair and A. Kudrolli, Phys. Rev. E **67**, 021302 (2003).
[28] L. Oyarte, P. Gutiérrez, S. Aumaitre, and N. Mujica, Phys. Rev. E **87**, 022204 (2013).
[29] A. R. Abate and D. J. Durian, Phys. Rev. Lett. **101**, 245701 (2008).
[30] I. F. Sbalzarini and P. Koumoutsakos, J. Struct. Biol. **151**, 182 (2005).
[31] S. McNamara and S. Luding, Phys. Rev. E **58**, 813 (1998).
[32] S. McNamara and E. Falcon, Powder Technol. **182**, 232 (2008).
[33] C. R. K. Windows-Yule, A. D. Rosato, D. J. Parker, and A. R. Thornton, Phys. Rev. E **91**, 052203 (2015).
[34] W. Losert, D. G. W. Cooper, J. Delour, A. Kudrolli, and J. P. Gollup, Chaos **9**, 682 (1999).
[35] A. Barrat, E. Trizac, and J.-N. Fuchs, Eur. Phys. J. E **5**, 161 (2001).
[36] A. Barrat and E. Trizac, Eur. Phys. J. E **11**, 99 (2003).
[37] J. A. Perez, S. B. Kachuck, and G. A. Voth, Phys. Rev. E **78**, 041309 (2008).
[38] P. M. Reis, R. A. Ingale, and M. D. Shattuck, Phys. Rev. E **75**, 051311 (2007).
[39] P. Melby, F. V. Reyes, A. Prevost, R. Robertson, P. Kumar, D. A. Egolf, and J. S. Urbach, J. Phys.: Condens. Matter **17**, S2689 (2005).
[40] J. S. van Zon and F. C. MacKintosh, Phys. Rev. E **72**, 051301 (2005).
[41] C. Qiong and H. Mei-Ying, Chin. Phys. B **23**, 074501 (2014).
[42] J Mattsson, H. M. Wyss, A. Fernandez-Nieves, K. Miyazaki, Z. Hu, D. R. Reichman, and D. A. Weitz, Nature (London) **462**, 83 (2009).
[43] R. A. Bordallo-Favela, A. Ramírez-Saíto, C. A. Pacheco-Molina, J. A. Perera-Burgos, Y. Nahmad-Molinari, and G. Pérez, Eur. Phys. J. E **28**, 395 (2009).
[44] D. A. McQuarrie, *Statistical Mechanics* (University Science Books, Sausalito, CA, 2000).